

Results from Radiating Divertor Experiments with RMP ELM Suppression

T.W. Petrie 1), T.E. Evans 1), N.H. Brooks 1), M.E. Fenstermacher 2), J.R. Ferron 1), B. Hudson 3), A.W. Hyatt 1), T.C. Luce 1), C.J. Lasnier 2), S. Mordijck 4), R.A. Moyer 4), P.A. Politzer 1), M.E. Rensink 2), M.J. Schaffer 1), P.B. Snyder 1), and J.G. Watkins 5)

- 1) General Atomics, PO Box 85608, San Diego, California 92186-5608, USA
- 2) Lawrence Livermore National Laboratory, Livermore, California 94550, USA
- 3) Oak Ridge Institute for Science Education, Oak Ridge, Tennessee 37831, USA
- 4) University of California-San Diego. San Diego, California 92093-0417, USA
- 5) Sandia National Laboratories, Albuquerque, New Mexico 87185, USA

e-mail contact of main author: petrie@fusion.gat.com

Abstract. The range in density for which resonant magnetic perturbations (RMPs) is effective in suppressing edge-localized modes (ELMs) in the presence of a radiating divertor is found to be modest in DIII-D. In general, our results highlight the difficulty in maintaining ELM suppression at the higher plasma densities representative of a successful radiating divertor operation. When the deuterium and argon gas puff rates were increased, the density and the edge electron pedestal pressure gradient (∇P_e) also increased. Once ∇P_e reached values consistent with the peeling-ballooning stability limit, as determined by edge stability analysis, Type-1 ELMing activity re-emerged. Differences in argon accumulation in the main plasma between RMP and similar non-RMP ELMing H-mode plasmas were relatively small, with the RMP cases somewhat higher ($\sim 20\%$) in general. Similar reductions in the core concentration of injected argon with an increasing rate of deuterium injection were observed in both RMP and non-RMP cases, suggesting that the detailed UEDGE divertor and scrape-off layer analysis reported previously for non-RMP radiating divertor plasmas might also carry over to RMP cases. Even with the re-appearance of ELMing activity, a radiating divertor with RMP generated higher levels of total radiated power ($\sim 40\%$) than comparable standard ELMing discharges without RMP at the same density. Although complete ELM-suppression in RMP/puff and pump plasmas was only accessible over a limited range in pedestal density n_{PED} , significant ELM mitigation was still attainable over a much wider range in n_{PED} .

1. Introduction

The transient heat loads delivered to the divertor targets during edge-localized modes (ELMs) may result in severe material erosion that may compromise divertor integrity in future tokamaks [1]. Recent studies, however, have pointed to the feasibility of mitigating or even suppressing ELMs by applying resonant magnetic perturbations (RMPs) to the pedestal region of the plasma [2-4]. While the underlying physics of resonant magnetic perturbations remains a subject of investigation, RMPs offer at least an intriguing option for dealing with deleterious ELMing activity.

Although RMPs can be effective in eliminating *transient* heat damage from ELMs, the *non-transient* heating component at the divertor targets can still be unacceptably high. Previous studies have shown that a radiating divertor can effectively reduce and control the steady power flow to the divertor targets [5-8]. In particular, the ‘‘puff and pump’’ radiating divertor experiments in DIII-D have demonstrated significant reductions in power loading at the divertor targets with little degradation in favorable H-mode properties. Here, ‘‘seed’’ impurities were injected into the private flux region (PFR) and restrained from diffusing into the plasma core by a combination of deuterium gas injection upstream and active particle exhaust at the divertor target.

Hence, the RMP approach and the puff and pump approach each focus on distinct aspects of the divertor heat load issue. In this paper we examine whether or not RMP ELM suppression/mitigation can be successfully merged with the puff and pump radiating divertor approach in order to address both transient and non-transient power loading issues simultaneously. We specifically investigate their compatibility in maintaining ELM

mitigation/suppression as deuterium and impurity gases are added to the system, in minimizing the peak heat flux at the divertor targets, and in sustaining favorable core plasma properties during the discharge.

2. Experimental Arrangement

The unperturbed MHD equilibrium contour for the lower single-null (SN) used in this study is shown in Fig. 1. Active pumping of the injected deuterium (D_2) and argon (Ar) gases is done with a single cryopump located in the lower divertor plenum. The radial location of the outer divertor strike point (ROSP) is positioned next to the entrance of the lower divertor plenum for maximum pumping. Argon is injected directly into the PFR, while D_2 is injected into the crown of the lower single-null (SN) configuration to increase the deuterium ion flow toward the lower divertor pump. Argon was chosen as the seed impurity, because it radiates effectively at the temperatures representative of the divertor and pedestal regions in DIII-D H-mode plasmas and has a relatively short ionization mean-free path. Since the first wall and divertor armor are graphite, carbon is the dominant intrinsic impurity in DIII-D discharges. The plasmas in this study were characterized by: $I_p = 1.43$ MA, $B_T = 1.8$ T, $q_{95} \approx 3.5$, $P_{INJ} \approx 5.5$ -6.5 MW, $H_{98(y,2)} \approx 0.9$ -1.2, $\beta_N \approx 2$, $\bar{n}_e/n_{eG} \approx 0.3$ -0.7, $P_{RAD}/P_{INJ} \approx 0.3$ -0.8, $Z_{eff} \approx 1.8$ -2.5, and the direction of the ion $\mathbf{B} \times \nabla B$ drift was toward the X-point.

DIII-D has two off-axis rows of six internal coils each, the ‘‘I-coil’’, that are used for ELM suppression and mitigation experiments in an $n=3$ magnetic configuration [9]; the poloidal location of the two rows of coils are also shown in Fig. 1. The data presented in this paper employs the I-coil with $n=3$, 60° phasing in even parity. This means that the coils above and below the midplane at a given toroidal position are of the same polarity, i.e., up-down symmetric. For the maximum coil current of 6.0 kA, this results in a resonant surface-averaged perturbation strength δb_r of $\sim 6.5 \times 10^{-4}$ T in the pedestal region (i.e., $\Psi_N = 0.95$) [4]. Unless otherwise specified, the I-coil current used in this experiment was 5.8 kA.

3. Results

3.1. ELM-suppression During Gas Puffing

Figure 2 shows that RMP-induced ELM suppression diminished and ultimately was lost during D_2 and Ar injection phases [Figs. 2(a,b)]. The activation of the I-coils at $t = 2.0$ s resulted in an immediate decrease in the pedestal density n_{PED} from a pre-activation value of $n_{PED}/n_{eG} = 0.30$ (at $t = 1.9$ s) to a post-activation value of 0.15 (at $t = 2.7$ s). The ELMs were completely suppressed within 0.2 s of I-coil activation. Deuterium and Ar injection were initiated at 2.8 s and 3.2 s, respectively. With gas injection, pedestal density increased almost immediately [Figs. 2(b)], although pedestal electron temperature T_{PED} did not start to decrease until well afterward [Figs. 2(c)]. Following I-coil activation, the electron collisionality in the pedestal (ν_e^*) [10] and the maximum electron pressure gradient in the pedestal $\nabla P_{e,MAX}$ decreased sharply, but they partially recovered during the subsequent gas puffing [Figs. 2(d,e)]. (We note that $\nabla P_{e,MAX}$ within the pedestal was determined just prior to an

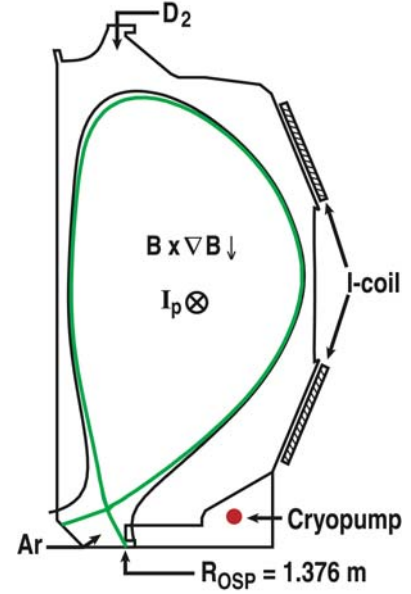


FIG. 1. The poloidal locations of the gas injectors, the divertor pumping plenum, and the RMP I-coil are shown together with the lower single-null cross-section of the unperturbed MHD configuration used in this study.

ELMing event.) The range in n_{PED} allowing ELM-suppressed operation was relatively small and it was largely insensitive to the various gas puff rates used in this experiment.

In Fig. 3, ν_e^* is plotted versus n_{PED} for the three the distinct phases of the H-mode discharges we wish to examine: (1) ELMing, (2) ELM transition, and (3) ELM-suppressed. While the ELMing and ELM-suppressed phases are self-explanatory, the *transition* phase refers to those parts of the discharge where sporadic ELMing occurred. During the ELMing phase before the I-coil is activated, the average n_{PED} is $\approx 0.40 \times 10^{20} \text{ m}^{-3}$. Shortly after I-coil activation, ELM-suppression was largely found in the range $n_{\text{PED}} \approx (0.17-0.25) \times 10^{20} \text{ m}^{-3}$, a *transition* interval for $n_{\text{PED}} \approx (0.25-0.30) \times 10^{20} \text{ m}^{-3}$, and ELMing regime for $n_{\text{PED}} > 0.30 \times 10^{20} \text{ m}^{-3}$. In these plasmas, ELM-suppression was observed when $\nu_e^* < 0.3$, the ELM transition with $\nu_e^* \approx 0.3-0.45$, and the ELMing regime with $\nu_e^* > 0.45$. At this time, the precise role of pedestal electron collisionality in the reappearance of ELMing is not altogether clear. Perhaps changes in ν_e^* due to fueling effects may alter the pedestal stability limits, as suggested in [11–13].

Figure 4 shows that, as $\nabla P_{e,\text{MAX}}$ increased with pedestal density, ELM-suppressed plasmas evolved into solidly ELMing H-mode discharges. Analysis using the ELITE edge plasma stability code [14] suggests that peeling-ballooning mode instabilities trigger the onset of these Type-1 ELMs. From this standpoint, it is not surprising that, as pedestal $\nabla P_{e,\text{MAX}}$ increased, ELMing activity should re-emerge.

RMP ELM suppression was attempted in similarly-configured plasmas where the ion $\mathbf{B} \times \nabla B$ drift was directed *away from the X-point*. For these plasmas, the levels of ν_e^* that were reached were clearly within the ELM suppression regime for the plasmas discussed in Fig. 3 (e.g., ≈ 0.25) but yet continuous ELMing was still observed. In fact, for the cases we investigated, we found no I-coil current that would suppress ELMing activity while still maintaining the H-mode confinement. We speculate that, even though there was similar power input in both drift direction cases, the “away” cases were operating closer to the L-H power threshold than the standard “toward” cases, and this may have played a role. Why the RMP suppression is so different from the $\mathbf{B} \times \nabla B$ drift direction is reversed is an open question that is under review.

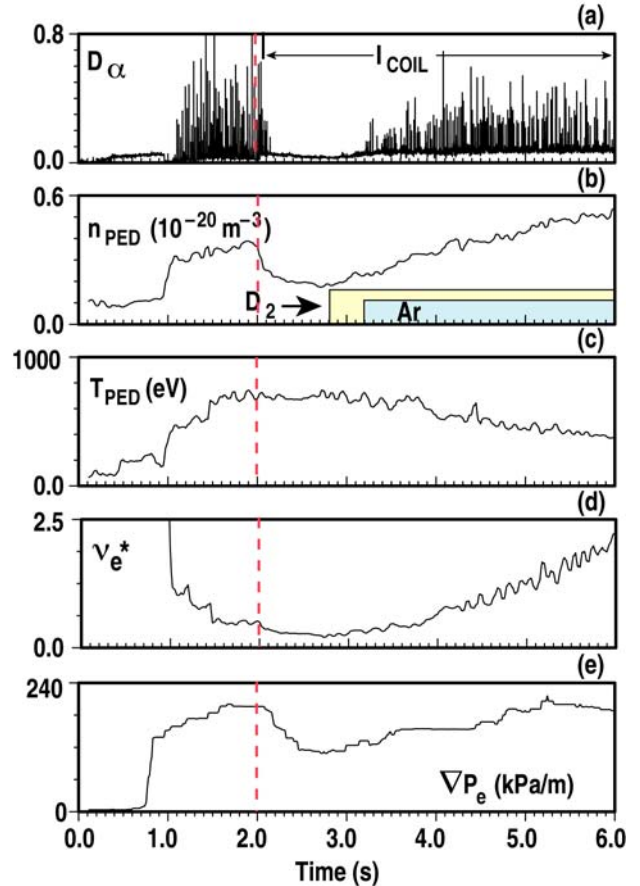


FIG. 2. The re-emergence of ELMing activity during deuterium and argon injection. (a) Deuterium recycling D_α , (b) pedestal density n_{PED} , (c) pedestal T_{PED} , (d) pedestal electron collisionality ν_e^* , and (e) $\nabla P_{e,\text{MAX}}$. Note that the I-coil is activated at $t = 2.0$ s (dotted vertical line) and that the argon (shaded blue) and the deuterium (shaded yellow) boxes in (b) represent only their injection times and are not their absolute ratios. $\Gamma_{\text{D}_2} = 10 \text{ Pa m}^3/\text{s}$ and $\Gamma_{\text{Ar}} = 0.05 \text{ Pa m}^3/\text{s}$.

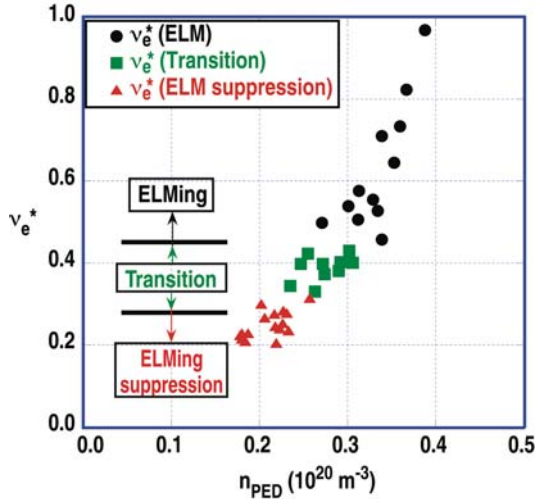


FIG. 3. Electron collisionality in the pedestal is plotted vs n_{PED} . $\Gamma_{D2} = 0-10 \text{ Pa m}^3/\text{s}$ and $\Gamma_{Ar} = 0.05 \text{ Pa m}^3/\text{s}$.

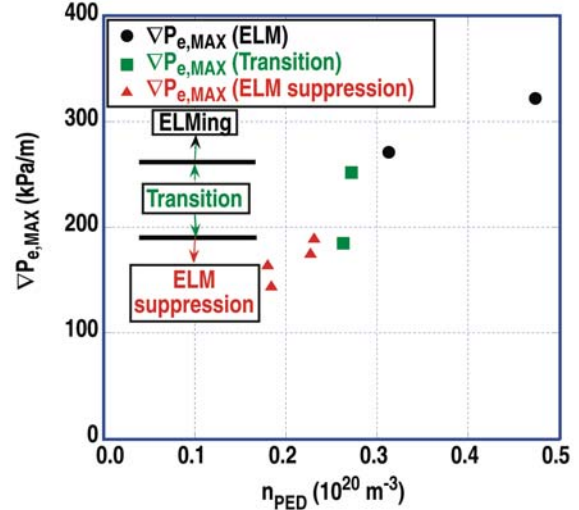


FIG. 4. The maximum electron pressure gradient in the pedestal is plotted vs n_{PED} . $\Gamma_{D2} = 0-10 \text{ Pa m}^3/\text{s}$ and $\Gamma_{Ar} = 0.05 \text{ Pa m}^3/\text{s}$. The ELM, ELM-transition, and ELM-suppression regimes are shown.

3.2 Argon Accumulation in the Main Plasma

The application of RMP to ELMing H-mode plasmas affects density, energy confinement, and impurity accumulation. An example of this is shown in Fig. 5 for three I-coil current values (0, 3.2, and 5.8 kA); complete ELM suppression was achieved for the 3.2- and 5.8-kA cases. The same trace amount of argon and power input [Fig. 5(a,b)] was applied in each case but there was no deuterium injection. As expected, the application of the I-coil at $t = 2.0 \text{ s}$ was accompanied by density pump-out, although it is interesting that, in the I-coil range investigated here, there was little difference in the density pump-out between 3.2 kA and 5.8 kA [Fig. 5(c)]. On the other hand, the energy confinement factor $H_{98(y,2)}$ decreased as the I-coil current was increased [Fig. 5(d)]; even with I-coil activated, H-mode energy confinement still remained substantial, i.e., $H_{98(y,2)} \approx 1.25$ (at I-coil = 0), ≈ 1.00 (at 3.2 kA), and ≈ 0.88 (at 5.8 kA) at $t = 5.8 \text{ s}$. For these shots, the buildup in argon density was 20%-25% higher for plasmas with the I-coil activated [Fig. 5(e)]. Interestingly, there was little change in argon accumulation between the 3.2 kA and 5.8 kA cases.

Figure 6 shows the differences in argon accumulation inside the main plasma between RMP and similar non-RMP ELMing H-mode

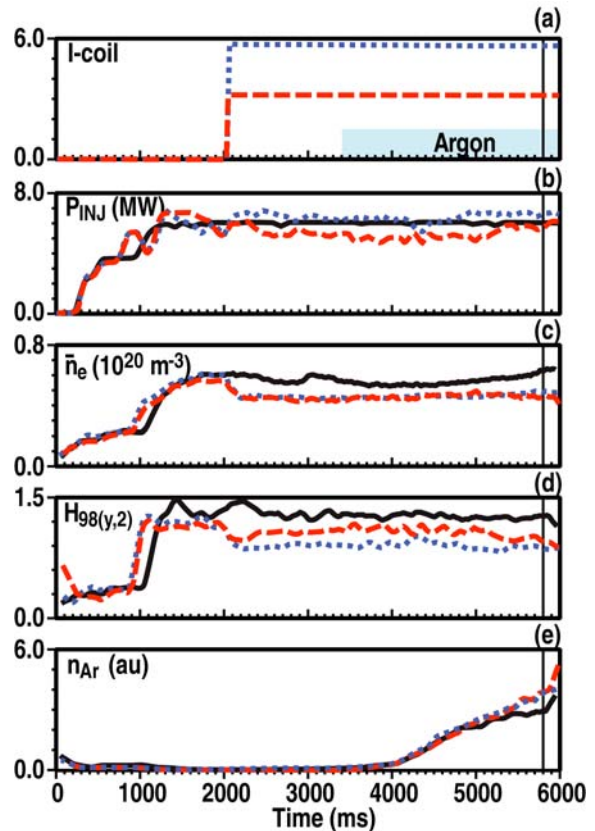


FIG. 5. The behavior of key plasma properties under (a) three values of I-coil current: 0, 3.2, and 5.8 kA, (b) P_{INJ} , (c) \bar{n}_e , (d) $H_{98(y,2)}$, and (e) relative core argon accumulation (n_{Ar}). For these cases, $\Gamma_{Ar} = 0.05 \text{ Pa m}^3/\text{s}$ and $\Gamma_{D2} = 0 \text{ Pa m}^3/\text{s}$.

plasmas as a function of the deuterium injection rate Γ_{D_2} . As with the non-RMP cases, we found that the core concentration of argon in the RMP cases decreased with increasing Γ_{D_2} . Figure 6 suggests that many of the physical processes detailed in UEDGE [15] fluid transport modeling reported previously for non-RMP radiating divertor plasmas [8] may also be important in these corresponding RMP cases, e.g., the importance of particle drifts in “fueling” the core plasma and screening the argon from the core plasma. This is a key point, because the extensive studies in optimizing the performance of radiating divertor plasmas in *non-RMP* cases provide direction as to how radiating divertor cases *with RMP* might be optimized. The return of Type-1 ELMing activity at the higher gas puff rates (or higher n_{PED}) in RMP plasmas may be responsible for the similarity in argon impurity accumulation in the main plasma between RMP and non-RMP discharges. UEDGE modeling of these RMP plasmas is underway.

3.3. Radiating Divertor with RMP

The operating space in density for complete ELM suppression by RMP was somewhat limited for the parameters used in the puff and pump scenario discussed in Sec. 3.1. Even without complete ELM suppression, however, significant mitigation of the effect of ELM pulses at the divertor targets is still possible over a broad operating range. Pedestal density dropped almost a factor of two following I-coil activation at $t = 2.0$ s, but increased to 25% above its pre-RMP value by the end of the shot after steady deuterium and argon gas puffing was added [Fig. 7(a,b)]. T_{PED} was unchanged after the I-coil was activated [Fig. 7(b)]; more detailed analysis has shown that the entire T_e -profile itself was unchanged after the I-coil activation. Pedestal electron temperature began to decrease about one second after deuterium gas puffing was turned on.

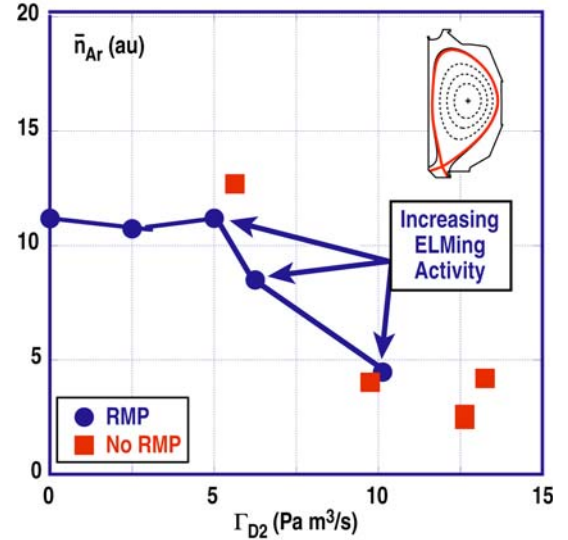


FIG. 6. Relative core argon accumulation in the core plasma (\bar{n}_{Ar}) as a function of Γ_{D_2} , in both RMP and non-RMP radiating divertor discharges. The methodology in determining \bar{n}_{Ar} is described in Ref. [16]. $\Gamma_{Ar} = 0.05 \text{ Pa m}^3/\text{s}$ in all cases.

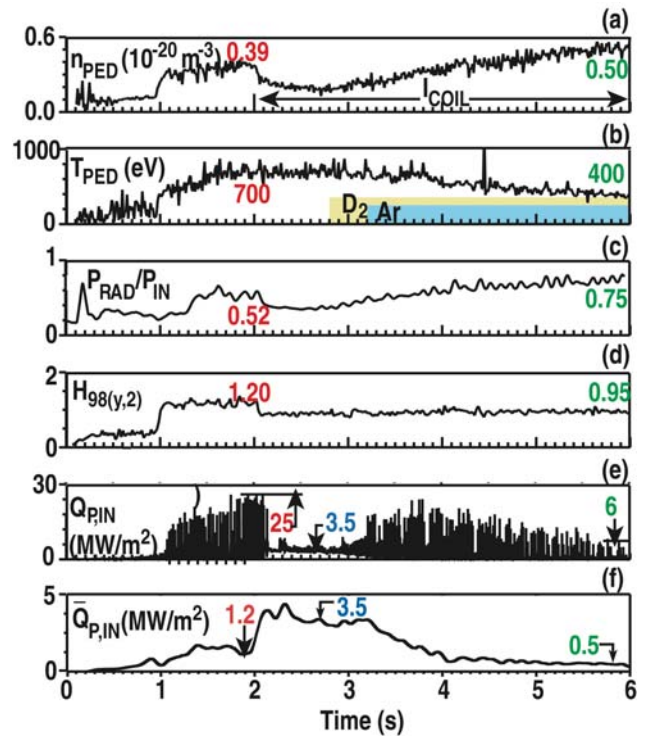


FIG. 7. (a) n_{PED} , (b) T_{PED} , (c) radiative fraction P_{RAD}/P_{IN} , (d) $H_{98(y,2)}$, (e) instantaneous inner divertor peak heat flux $Q_{P,IN}$, and (f) time-averaged peak heat flux $\bar{Q}_{P,IN}$. Numerical values of the quantities described in each box are shown at various points in the discharge. Plasma parameters: $I_p = 1.43 \text{ MA}$, $q_{95} = 3.5$, and $P_{IN} = 6.0 \text{ MW}$.

The ratio of radiated power to input power ($P_{\text{RAD}}/P_{\text{INJ}}$) decreased by about a third after the I-coil was activated but increased again during the D₂ and Ar injection phase, reaching ≈ 0.75 by the end of the shot [Fig. 7(c)]. ($P_{\text{RAD}}/P_{\text{IN}}$) was found to be $\approx 40\%$ greater under RMP puff and pump (RMP/PP) operation than for the corresponding standard ELMing H-mode (SEH) plasmas at the *same* n_{PED} . In this comparison, approximately one-third of this increase occurred in the SOL and divertor regions and two-thirds of this increase in the main plasma. The increase in the SOL and divertor radiated power was largely due to the higher puffing rates of deuterium (and argon “seed” impurity) required to maintain the pedestal density (i.e., in this case, $n_{\text{PED}} \approx 0.4 \times 10^{20} \text{ m}^{-3}$) after the I-coil was activated. In turn, this produced a higher SOL density and lower plasma temperatures in both the plasma edge and SOL/divertor that favored higher radiated power. The increase in the radiated power in the main plasma was largely due to the accumulation of argon and a 10%-15% reduction in T_{PED} . While $H_{98(y,2)}$ was reduced $\approx 25\%$ after the I-coil was activated, the energy confinement time during subsequent deuterium and argon puffing continued to be representative reasonable H-mode confinement [i.e., $H_{98(y,2)} \approx 0.9$] and was insensitive to changes in n_{PED} [Fig. 7(d)]. The above suggests that with a proper combination of RMP and gas puffing, active control of density over a wide range is achievable while still maintaining reasonable H-mode confinement.

The temporal history of the *peak heat flux* deposited at the inner divertor target ($Q_{\text{P,IN}}$) is shown in Fig. 7(e). The “spikes” indicate the transient heat flux behavior during ELMing activity, which was observed throughout the H-mode except for the one-second interval following RMP activation. When ELMing re-appeared during the gas puffing phase, $Q_{\text{P,IN}}$ did not return to values prior to I-coil activation. For example, after n_{PED} had regained its pre-RMP value near $t = 4.6$ s, $Q_{\text{P,IN}}$ was reduced $\approx 30\%$ compared with pre-RMP times. When n_{PED} was raised further, the peak ELM heat flux was reduced by $\approx 60\%$ - 70% , compared with $Q_{\text{P,IN}}$ prior to RMP.

The application of RMP eliminated Type-1 ELMs, as well as the transient high peak heat fluxes $Q_{\text{P,IN}}$ associated with them. However, the *time-averaged* peak heat flux ($\bar{Q}_{\text{P,IN}}$) *increased* by almost a factor of three after the I-coil was activated [Fig. 7(f)]. Raising n_{PED} and radiated power by gas puffing reduced $\bar{Q}_{\text{P,IN}}$, but the ELMs and their high transient heat fluxes returned. Ultimately, raising n_{PED} resulted in $Q_{\text{P,IN}}$ fading, particularly after the inner divertor leg detached between ELM pulses (i.e., $t \approx 4.0$ s).

In general, we have found that applying RMP to the puff and pump approach can affect $Q_{\text{P,IN}}$ and $\bar{Q}_{\text{P,IN}}$ differently, as shown in Fig. 8(a,b). For example, by eliminating ELMs in the absence of gas puffing, the “RMP only” approach reduced $Q_{\text{P,IN}}$ by a factor ≈ 6 [Fig. 8(a)], but yielded the highest $\bar{Q}_{\text{P,IN}}$ [Fig. 8(b)]. When the density was raised, the plasma began again to ELM, although these ELMs in the “transition” regime (Sec. 3.1) generally had lower $Q_{\text{P,IN}}$ than either those that occurred at slightly higher pedestal densities or those that occurred prior to RMP activation. Figure 8(b) also shows that between-ELM detachment of the inner divertor leg during RMP/PP operation occurred at the about the same n_{PED} as prior to I-coil initiation, which at that time was still largely attached between ELMs. This drop in density with RMP, along with the gas puffing needed to restore the pre-RMP density enhanced the overall radiated power at the plasma edge and in divertor, and this, in turn, promoted detachment at a lower density than that which would occur in comparable SEH plasmas.

4. Discussion

ELMing activity in these plasmas ceased shortly after RMP was applied, and n_{PED} , v_e^* , and $\nabla P_{e,\text{MAX}}$ in the pedestal were all reduced $\approx 50\%$. When D₂ and Ar gases were injected, continuous ELMing eventually re-emerged, although n_{PED} , v_e^* and $\nabla P_{e,\text{MAX}}$ had only recovered $\approx 70\%$ - 80% of their pre-RMP values. Because ELITE code analysis suggests that

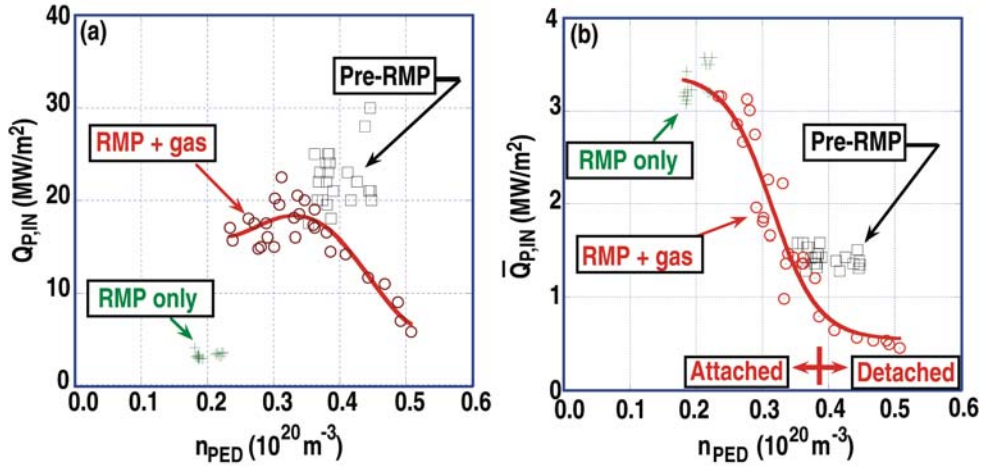


FIG. 8. (a) $Q_{P,IN}$ and (b) $\bar{Q}_{P,IN}$ are plotted as a function of n_{PED} during the three stages of RMP/radiating divertor discharges discussed in the text.

peeling-ballooning mode instabilities may be triggering the re-appearance of ELMs, the observed increases in ∇P_e during “recovery” could be associated with making the pedestal more susceptible to ELMs. Figures 3 and 4 suggest that the “headroom” in v_e^* and $\nabla P_{e,MAX}$ between ELM-suppressed and ELM re-emergence is relatively narrow for these plasmas.

Successful ELM suppression by RMP clearly puts a limit on Γ_{D2} (and Γ_{Ar}) that is available for the puff and pump operation. Previous studies of the puff and pump approach at DIII-D have shown that higher Γ_{D2} leads to better screening of the seed impurity from the main plasma [7]. The “best” puff and pump results for the plasmas described here would require $\Gamma_{D2} \approx 12\text{-}13$ Pa m³/s, which is considerably above the maximum allowed Γ_{D2} for complete ELM-suppression (i.e. <3.5 Pa m³/s). While a higher particle pumping rate would be helpful in raising this maximum allowed Γ_{D2} , the above results highlight the challenges for future devices in combining RMP-based ELM suppression with optimal puff and pump radiating divertor.

Our results indicate that ELM *mitigation* at higher density and gas puffing rates may be more readily-attained than complete ELM *suppression*. While much of our initial focus of this study was directed toward complete ELM-suppression via RMP during radiating divertor operation, our results show that complete ELM suppression with RMP may not be necessary (or even advisable, in some cases) to deal successfully with heat flux at the divertor targets. This is due to there being two distinct components of the divertor heat flux, i.e., the transient $Q_{P,IN}$ (driven largely by ELMs) and the time-averaged $\bar{Q}_{P,IN}$. By applying RMP *without* gas puffing to an ELMing plasma, we observed the expected major reduction in $Q_{P,IN}$, such that $Q_{P,IN} \approx \bar{Q}_{P,IN}$. At the same time, however, $\bar{Q}_{P,IN}$ was higher than for any other times before RMP was applied or after gas puffing was initiated. We found that we could reduce $\bar{Q}_{P,IN}$ by a combination of deuterium and argon gas puffing. The cost of doing this, however, was triggering the return of ELMs, although at a lower transient $Q_{P,IN}$ than pre-RMP. For example, a $\approx 30\%$ higher radiative fraction in RMP/PP plasmas over comparable SEH plasmas at the same n_{PED} yielded a roughly 30% drop in $Q_{P,IN}$. Further gas puffing led to higher n_{PED} and radiative fractions, which reduced both transient and time-averaged peak heat fluxes much further below pre-RMP values. An important point here is to note that once RMP had been activated, there was little further degradation in the energy confinement time as the pedestal density was raised during puff and pump operation.

The results discussed in this paper suggest possibilities for improved RMP/PP operation. One approach is based on enhancing the particle exhaust by exploiting what we learned in previous (non-RMP) puff and pump experiments, particularly with regard to how particle

drifts affect pumping effectiveness. In the plasma discussed here, particle pumping was done only on the outer divertor leg with the ion $\mathbf{B} \times \nabla B$ drift directed toward the X-point. While this arrangement has been successful in suppressing ELMs, compared with the other pumping configurations available on DIII-D, this arrangement is least effective in controlling particle inventory and fueling of the main plasma, and hence in maintaining the lower density (and collisionality) conditions favorable to ELM suppression. Based on previous work in non-RMP radiating divertors [8], the most effective way to control particle inventory (and preserve RMP ELM suppression) would be to maximize the divertor pumping and to operate with the ion $\mathbf{B} \times \nabla B$ drift directed away from the X-point. For DIII-D, this would mean SN operation in the closed upper divertor which has much stronger pumping, i.e., two cryopumps available, with the ion $\mathbf{B} \times \nabla B$ drift directed away from the X-point. However, from our discussion in Sec. 3.1, this approach necessitates that we understand why RMP-based ELM suppression has been so much more difficult to achieve than with the ion $\mathbf{B} \times \nabla B$ drift directed toward the X-point. Another area of investigation that is worth examining is to set-up the I-coil arrangement in odd parity, instead of the even parity used in this study.

A more speculative approach focuses on inhibiting the buildup of pedestal ∇P_e , since our results in Sec. 3.1 suggest that the increase in pedestal ∇P_e enhances the chance of triggering an ELM. One might do this by directing ECH absorption to the pedestal. ECH applied to plasma edge may enhance particle transport near the maximum in ∇P_e and thus inhibit the building of ∇P_e .

5. Final Considerations

Our study provides a first step toward understanding RMP ELM suppression/mitigation physics under radiating divertor conditions. However, it is not possible in present day tokamaks to produce pedestal parameters that match the non-dimensional plasma parameters of an ITER-like device, while at the same time producing a radiating divertor that matches the radiating divertor parameters of this device. Such mismatches can affect how RMP ELM-suppressed H-modes would couple to a radiating divertor in an ITER-type device. Thus, it is prudent at this time to be cautious in extrapolating our results to future tokamaks.

This work was supported by the US Department of Energy under DE-FC02-04ER54698, DE-AC52-07NA27344, DE-AC05-06OR23100, DE-FG02-07ER54917, DE-FG02-05ER54809, and DE-AC04-94AL85000.

References

- [1] FEDERICI, G., et al., Plasma Phys. Control. Fusion **45** (2003) 1523.
- [2] EVANS, T.E., et al., Phys. Rev. Lett. **92** (2004) 235003.
- [3] LIANG, Y., et al., Plasma Phys. Control. Fusion **49** (2007) B581.
- [4] EVANS, T.E., et al., Nucl. Fusion **48** (2008) 024002.
- [5] RAPP, J., et al., Nucl. Fusion **44** (2004) 312.
- [6] KALLENBACH, A., et al., J. Nucl. Mater. **337-339** (2005) 732.
- [7] PETRIE, T.W., et al., J. Nucl. Mater. **363-365** (2007) 416.
- [8] PETRIE, T.W., et al., Nucl. Fusion **48** (2008) 045010.
- [9] EVANS, T.E., et al., Phys. Plasmas **13** (2006) 056121.
- [10] SAUTER, O., et al., Phys. Plasmas **6** (1999) 2834.
- [11] SNYDER, P.B., et al., Nucl. Fusion **47** (2007) 961.
- [12] THOMAS, D.M., et al., Plasma Phys. Control. Fusion **48** (2006) A183.
- [13] FENSTERMACHER, M.E., et al., J. Nucl. Mater. **363-365** (2007) 476.
- [14] SNYDER, P.B., et al., Phys. Plasmas **9** (2002) 2037.
- [15] ROGNLIEN, T.D., et al., J. Nucl. Mater. **196-198** (1992) 347.
- [16] PETRIE, T.W., et al., Nucl. Fusion **49** (2009) 065013.